Confined Discotic Liquid Crystalline Self-Assembly in a Novel Coil−Coil−Disk Triblock Oligomer

Li Cui,[†] Jianjun Miao,[†] Lei Zhu,[*,†] Igors Sics,[‡] and Benjamin S. Hsiao[‡]

Polymer Program, Institute of Materials Science and Department of Chemical Engineering, The University of Connecticut, Storrs, Connecticut 06269-3136, and Chemistry Department, State University of New York at Stony Brook, Stony Brook, New York 11794-3400

Received November 22, 2004; Revised Manuscript Received January 31, 2005

ABSTRACT: An asymmetric ABC coil−coil−disk triblock oligomer, based on polyethylene-*block*-poly(ethylene oxide)-*block*-pentakis(pentyloxy)triphenylene (PE-*b*-PEO-*b*-P5T or EEO−P5T), was successfully synthesized by coupling a hydroxyl-terminated PE-*b*-PEO diblock oligomer and 2-hydroxy-3,6,7,10,11-pentakis(pentyloxy)triphenylene using oxalyl chloride. The structure and morphology of the supramolecular self-assembly in bulk EEO−P5T were studied by differential scanning calorimetry, small- and wide-angle X-ray scatterings, polarized light microscopy, and transmission electron microscopy. The PE block crystallized into interdigitated, extended chain crystals with a chain-tilting angle of 23° from the lamellar normal. The peak melting temperature (T_m) of the PE crystals was at 93.8 °C. The PEO block remained in the amorphous state because of its both ends being tethered to other two blocks and the mismatch of the cross-section areas at the PE−PEO and PEO−P5T interfaces. Bilayer P5Ts, sandwiched between amorphous PEO layers, exhibited a nematic columnar (N_{col}) to nematic discotic (N_D) transition at ca. 23 °C. Intriguingly, the N_D to isotropic (or vice versa) transition was observed to coincide with the melting (or crystallization) of the PE block.

Introduction

Self-assembly is a powerful protocol for predictable formation of nanostructures in supramolecular materials.[1] The process involves the formation of discrete ensembles of molecules, supermolecules, and nanoparticles into extended ordered arrays, such as crystals, liquid crystals, and colloids. The mobility in the form of large-amplitude motions of molecules enables them to find energy minimum in a thermodynamically driven self-assembly pathway. Understanding the fundamental physics of the self-assembly behavior in soft condensed matters has accounted for recent developments for the bottom-up strategy in nanoscience and nanotechnology.[2]

An important feature of supramolecular materials is the amphiphilicity, namely, at least two chemically different and physically incompatible molecular parts are linked together through covalent bonds. Because of the covalent connectivity, macroscopic phase separation is hindered and microphase separation occurs on nanometer scales. Typical examples for such ordered supramolecular assemblies include thermotropic[3] and lyotropic mesophases of surfactants,[4] ordered structures of polyelectrolyte−surfactant complexes,[5] and smectic, columnar, and cubic liquid crystalline phases and self-assembled morphologies of block copolymers.[6]

Among block copolymers, rod−coil block copolymers represent a unique class, where various hierarchical self-assemblies at different compositions have been observed experimentally.[7] For example, smectic C (SmC) type phases, such as wavy lamellar, zigzag morphology, bilayer SmC_2 phases with alternating synclinic−anticlinic interlayer correlation, and interdigitated arrowhead morphologies (intercalated anticlinic SmC phases) have been found in poly(*n*-hexyl isocyanate)-*b*-polystyrene (PHIC-*b*-PS) rod−coil diblock copolymers with an increase in the volume fraction of the rigid PHIC block.[8] Several different AB rod−coil as well as ABA and ABC coil−rod−coil molecules, containing rigid aromatic units and ethylene oxide or propylene oxide chains, exhibited smectic A (SmA), SmC, columnar phases, body-centered-cubic sphere phases, and even bicontinuous cubic phases such as double gyroid.[9] An unprecedented self-organization was suggested by Stupp for coil−coil−rod ABC triblock molecules,[10] which can self-assemble into mushroom-shaped nanostructures, lacking a center of symmetry. These “mushrooms” further organized into noncentrosymmetric polar monolayer structures. Jenekhe reported on the self-assembly behavior of rod−coil diblock copolymers consisting of poly(phenylquinoline) as the rod block and PS as the coil block.[11] Novel aggregates in the forms of hollow spheres, lamellar, hollow cylinders, and vesicles in a selective solvent for the rod segment were observed. Polystyrene-*block*-poly(*p*-phenylene) was synthesized by Francois et al.[12] Special nonequilibrium honeycomb morphologies, in which monodisperse pores arranged in a hexagonal array by evaporating the solvent from CS_2 solution in moist air, were observed.

Oligomeric block copolymers containing discotic mesogens have not been studied as extensively as calamitic liquid crystalline block copolymers. Selected studies are described as the following. A side-chain discotic liquid crystalline block copolymer of 2,6,7,10,11-pentapentyloxy-3-(3-acryloylpropyloxy)triphenylene (PPAT) and *tert*-butyl acrylate (*t*-BA) was synthesized by atom transfer radical polymerization (ATRP).[13] Hexagonal columnar mesophases were observed for different PPAT contents in the block copolymers. Another side-chain discotic liquid crystalline block copolymer was obtained by ionic complexation between poly(ethylene oxide)-*block*-poly(L-lysine) (PEO−PLL) and carboxylic acid containing

---

[†] The University of Connecticut.

[‡] State University of New York at Stony Brook.

[*] Corresponding author: e-mail lei.zhu@uconn.edu; Tel 860-486-8708.

10.1021/ma047590w CCC: $30.25

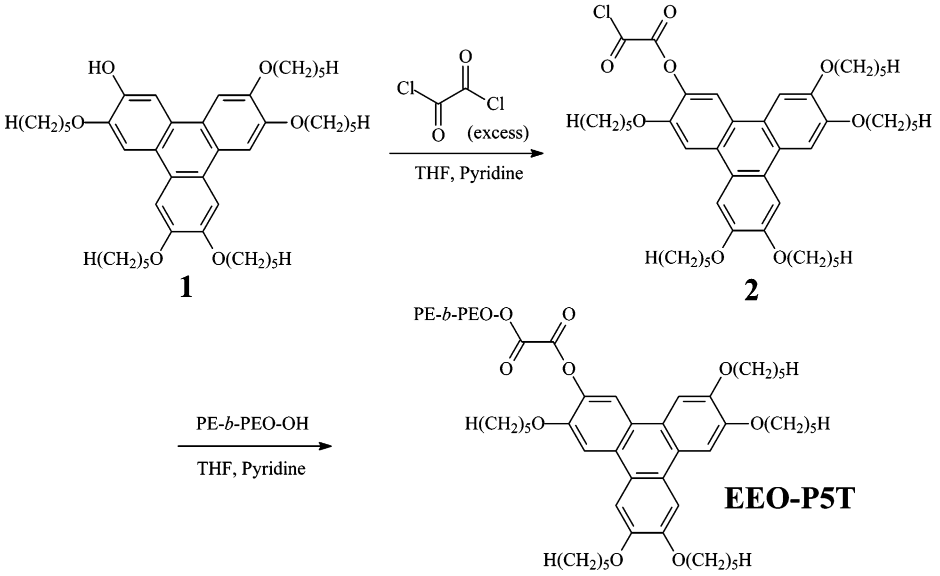

Scheme 1. Synthetic Scheme of EEO−P5T

hexaperihexabenzocoronene (HBC).[14] The α-helices of PLL main chains were surrounded by six discotic HBCs to form a hexagonal superlattice.

Recently, in a main-chain discotic liquid crystalline triblock copolymer, both ends of the middle triphenylene block were end-capped with PEO blocks having a molecular weight of 2000 g/mol.[15] At room temperature, the PEO blocks crystallized into crystalline lamellar, and the triphenylene blocks formed hexagonal columnar liquid crystalline phase. The column axes were oriented perpendicular to the crystalline lamellar normal. Above 60 °C, PEO crystals melted into hexagonal cylinders surrounded by the main-chain triphenylene blocks. The liquid crystalline hexagonal columns were aligned parallel to the amorphous PEO cylinders. Another main-chain jacketed liquid crystalline block copolymers, poly{styrene-*block*-(2,5-bis-[4-methoxyphenyl]oxycarbonyl)styrene} (PS−PMPCS), were synthesized by 2,2,6,6-tetramethyl-1-piperidinyloxy (TEMPO)-mediated living free radical polymerization.[16] It was found that PMPCS blocks formed supramolecular columnar nematic phase (N_{col}) within the lamellar block copolymers. Two layers of liquid crystalline columns were confined in each liquid crystalline domain with the columnar axes parallel to the block copolymer lamellar normal.

Oligomeric coil−disk type diblock copolymers have been investigated by McKeown et al.[17] In these systems, a phthalocyanine disk was linked to a single PEO chain with different molecular weights. When the PEO molecular weight was low, a hexagonal columnar phase was observed. However, when the PEO molecular weight exceeded 2200 g/mol, an $\mathrm{N_{col}}$ phase was observed and was attributed to the steric disturbance of the two-dimensional hexagonal lattice by the polymeric substituent.

In this work, an asymmetric ABC coil−coil−disk triblock oligomer, namely, polyethylene-*block*-poly(ethylene oxide)-*block*-pentakis(pentyloxy)triphenylene (PE-*b*-PEO-*b*-P5T, or EEO−P5T), was synthesized by coupling a hydroxyl-terminated PE-*b*-PEO (EEO) diblock oligomer and 2-hydroxy-3,6,7,10,11-pentakis(pentyloxy)triphenylene using oxalyl chloride. The number-average molecular weights (M_n's) for the PE and PEO blocks were 827 and 896 g/mol, respectively. The molecular weight of P5T was 731 g/mol (including the oxalate group). The self-assembly morphology in bulk EEO−P5T was studied using two-dimensional (2D) small-angle X-ray scattering (SAXS) and wide-angle X-ray diffraction (WAXD), polarized light microscopy (PLM), and transmission electron microscopy (TEM). The PE block was crystalline and had a melting temperature (T_m) of 93.8 °C. Unlike in the EEO diblock oligomer, the PEO block in EEO−P5T was amorphous. Interestingly, the P5T showed an isotropic to nematic discotic ($\mathrm{N_D}$) phase transition only when the PE blocks crystallized into lamellar structures. Upon further cooling, the $\mathrm{N_D}$ to nematic columnar (N_{ϕ}) transition was observed at ca. 23 °C for the bilayer P5T, confined between neighboring amorphous PEO layers.

Experimental Section

Materials. Tetrahydrofuran (THF) was refluxed with sodium/benzophenone for a couple of hours and was used immediately after distillation. Oxalyl chloride was freshly distilled before use. The nonionic surfactant, PE-*b*-PEO, was purchased from Aldrich Chemical Co., Inc. It had an average molecular weight of 1400 g/mol with a broad molecular weight distribution and 50 wt % PEO. A low molecular weight fraction with a narrow molecular weight distribution was obtained by fractionation.[18] From the end-group analysis using proton nuclear magnetic resonance (^{1}H NMR), the molecular weight of each block in the fractionated sample was 827 and 896 g/mol for the PE and PEO blocks, respectively. The molecular weight distribution determined by size-exclusion chromatography (SEC) was 1.08, using polystyrene as standards and THF as solvent. 1,2-Bis(pentyloxy)benzene was prepared according literature.[19] 2,3,6,7,10,11-Hexakis(pentyloxy)triphenylene was prepared by trimerization of 1,2-bis(pentyloxy)benzene using ferric chloride as oxidative agent.[20] 2-Hydroxy-3,6,7,10,11-pentakis(pentyloxy)triphenylene (**1** in Scheme 1) was prepared by cleavage of 2,3,6,7,10,11-hexakis(pentyloxy)triphenylene with 1.2 equiv of B-bromocatecholborane.[21] The other commercially available chemicals were used without further purification.

Synthesis of EEO−P5T. The synthetic route is shown in Scheme 1. A solution of 404 mg (0.6 mmol) of **1** in 5 mL of dry THF was added into a mixture containing 760 mg (6 mmol) of oxalyl chloride and 316 mg (4 mmol) of pyridine in 5 mL of THF. The reaction mixture was refluxed for 4 h, and the volatiles were evaporated under vacuum (ca. 25 mTorr). 475 mg (6 mmol) of pyridine in 5 mL of THF was added into the reaction flask, and 480 mg (0.3 mmol) of EEO in 10 mL of warm THF was added dropwise. The reaction mixture was refluxed for 4 h. After cooling to room temperature, the reaction mixture was poured into 120 mL of water. The precipitated solid was separated by centrifugation, dissolved in THF, and repeatedly precipitated in hexane and methanol twice. Finally, about 140 mg of EEO−P5T was obtained.

Instrumentation and Characterization. ^{1}H NMR spectra were recorded on a Bruker spectrometer (500 MHz, DMX 500). Molecular weight distribution was measured by SEC using a Waters system quipped with a refractive index detector. A mixture of DMF and chloroform (DMF:chloroform = 1:4) was used as eluent with a flow rate of 1.0 mL/min, and polystyrene standards were used for calibration. DSC experiments were carried out on a TA-2920 DSC instrument. Indium standard was used to calibrate the instrument. Approximately, 1 mg of sample was used for the DSC study, and the scanning rate was 5 °C/min.

2D simultaneous SAXS and WAXD experiments were performed at the X27C beamline in the National Synchrotron Light Source (NSLS), Brookhaven National Laboratory (BNL). The wavelength of the X-ray beam was 0.137 nm. The beam center was calibrated using silver behenate with the primary reflection peak at 1.076 nm^{-1}. The higher-order reflection peaks (up to 11th order) were used for WAXD calibration. Two Fuji imaging plates were used as SAXS and WAXD detectors. Typical data acquisition time was 1 min for both SAXS and WAXD measurements. Digital SAXS/WAXD images were obtained using a Fuji BAS-2500 scanner. The temperature-dependent X-ray experiments were performed using an Instec HCS410 hot stage, equipped with a liquid nitrogen cooling accessory. One-dimensional (1D) SAXS curves were obtained by integrating the corresponding 2D SAXS patterns. Azimuthal profiles were extracted from the 2D WAXD patterns with the zero-angle on the equator. The raw data were fitted with Gaussian functions in order to determine the position of peak maximum. The standard deviation in the peak position was estimated to be within ±3°.

The polarized light microscopy (PLM) experiments were performed using an Olympus BX51P microscope, also equipped with the Instec HCS410 hot stage. TEM experiments were performed on a Philips EM300 at an accelerating voltage of 80 kV. Thin sections with a thickness of ca. 75−100 nm were obtained using a Leica Ultracut UCT microtome equipped with a diamond knife at −50 °C. The thin sections were collected onto 400 mesh TEM grids, freeze-dried, and stained in RuO_4 vapor at room temperature for 20 min.[22]

Results and Discussion

Synthesis and Molecular Characterization. In the synthesis, **1** was added dropwise into 10 times excess oxalyl chloride to ensure monofunctionalization (Scheme 1). The intermediate **2** was not separated and purified before next step reaction. Two times excess of **2** over EEO−OH was used to ensure high coupling efficiency. After termination of the reaction, the excess **2** was removed by precipitation of the final product (in THF solution) into methanol several times. Column chromatography through acidic silica gel should be avoided, since the oxalate groups were found unstable even at room temperature in acidic column environment (ca. 10−20% decomposed into EEO and P5T after column chromatography). The purity of thus obtained product was checked by ^{1}H NMR (Figure 1) and was confirmed by thin-layer chromatography (TLC). All the peak assignments are indicated in Figure 1. The coupling efficiency was calculated from the ratio of peak **a** over peak **i** to be ca. 90%. The polydispersity (1.07) of EEO−P5T was obtained from SEC, as shown in Figure 2. Comparing with EEO diblock copolymer, the retention time for EEO−P5T shifted to a shorter time, indicating an increase in the hydrodynamic volume of the final product. We noticed that the polydispersity of EEO−P5T became slightly narrower than that of EEO.

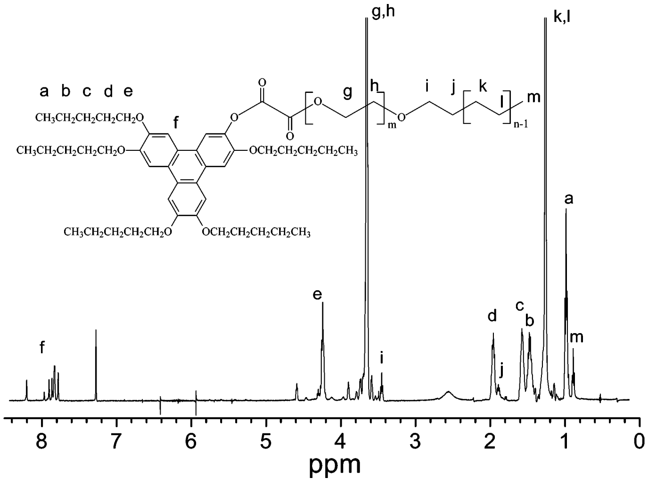

Figure 1. ^{1}H NMR spectrum of EEO−P5T in $CDCl_3$.

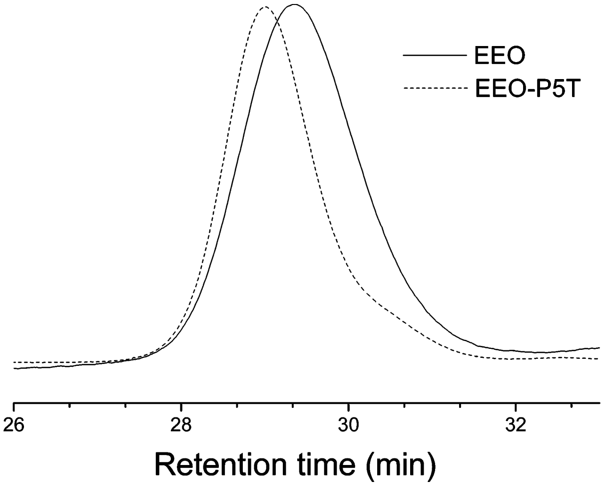

Figure 2. SEC curves of the diblock oligomer EEO and triblock copolymer EEO−P5T.

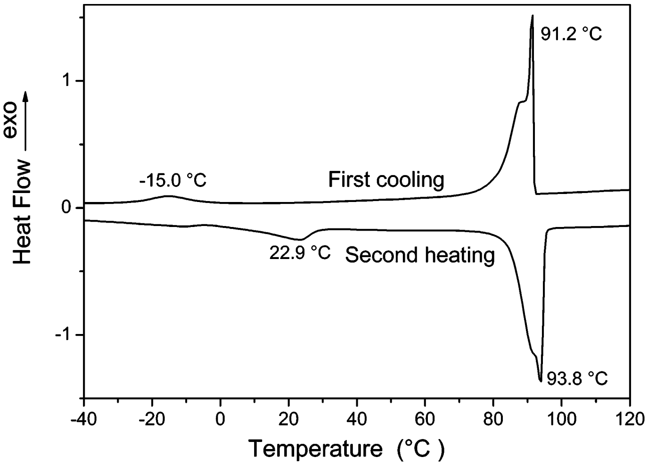

Figure 3. DSC curves of EEO−P5T at heating and cooling rates of 5 °C/min.

The thermal behavior of EEO−P5T is shown in the DSC thermogram in Figure 3. Two phase transitions were observed. Upon cooling, a major exotherm at 91.2 °C, representing the crystallization of PE blocks, and a weak exotherm (its onset temperature at −3.9 °C and peak temperature at −15 °C) were seen. Upon heating, a major endotherm at 93.8 °C, representing the melting of PE blocks, and a weak endotherm (its onset temperature at 5.8 °C and peak temperature at 22.9 °C) were

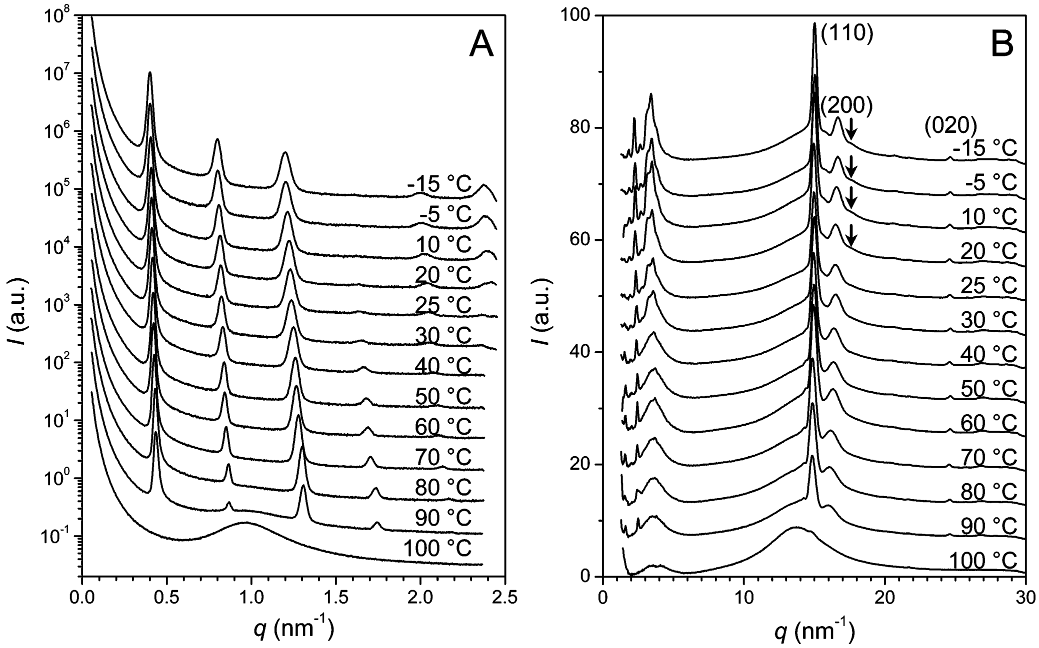

Figure 4. 1D SAXS (A) and WAXD (B) of EEO−P5T at different temperatures during a stepwise cooling process.

seen. The heat of fusion for the low-temperature transition was 13.1 J/g, and the heat of fusion of the PE crystals was 81 J/g. After normalization to the weight fraction, the true heat of fusion for the PE crystals was 243 J/g. The heat of fusion for perfect PE oligomers was 299 J/g as reported in a previous paper.[18b] The crystallinity of the PE block in EEO−P5T was thus 81.1 wt %. We note that double melting/crystallization peaks are observed around 92 °C in the DSC curves. Even after peak deconvolution, the transition enthalpy for each peak is still too high to be identified as a nematic liquid crystalline transition.[23] Here, we speculate that the double-melting peak for the PE crystals may be a consequence of inhomogeneity in the PE blocks such as a distribution in molecular weight and possible EEO diblock contamination. A detailed explanation needs further investigation.

Phase Transitions Studied by One-dimensional (1D) Simultaneous SAXS and WAXD. To identify the phase transitions observed by DSC, simultaneous SAXS and WAXD experiments were carried out, and results are shown in Figure 4. The temperature was stepwise decreased from 100 °C, and at each temperature the sample was equilibrated for 5 min before X-ray measurements. Above 95 °C, an isotropic phase was observed since no birefringence was observable under PLM. The SAXS data in Figure 4A show a correlation hole scattering centered 0.96 nm^{-1}, indicating the morphology of a homogeneous disordered phase. This correlation hole scattering can be explained as an average periodicity of density fluctuations among different blocks. The WAXD profile in Figure 4 shows two broad halos at $q = 3.72$ nm^{-1} and $q = 13.7$ nm^{-1}. The low-angle halo (d-spacing = 1.69 nm) originates from the average electron density fluctuations between the weak "microphase separation" of the triphenylene disk and coil diblock copolymers. The high-angle halo (d-spacing = 0.46 nm) can be attributed to the average distance among the diblock random coil chains.

Below 90 °C, the PE blocks crystallize into orthorhombic crystals showing (110), (200), and (020) reflections at q = 15.1, 16.7, and 24.6 nm^{-1}, respectively (Figure 4B). After the PE block crystallizes, the intensity of the broad peak at $q = 3.65$ nm^{-1} becomes stronger. In Figure 4A, the SAXS profiles show ordered lamellar reflections with q ratios as 1:2:3:4:5, and even higher order scattering peaks are found in the low-angle region of WAXD (Figure 4B). The overall lamellar thickness gradually increases continuously from 14.4 toward 15.8 nm as the temperature decreases. This may result from the nonuniformity in the molecular weight distribution in such a low molecular weight oligomer, as reported before.[18b]

Below 20 °C, the low-angle scattering halo in Figure 4B becomes relatively sharper and stronger, which superposes with the higher order lamellar reflections from the oligoblock copolymer. Another subtle change is the development of a weak scattering peak, at a position indicated by the arrows in Figure 4B, and will be discussed later. When the temperature reaches −15 °C, no PEO reflections at q = 13.41 and 16.34 nm^{-1} are observed, indicating that the PEO blocks remain as amorphous. This can be attributed to its both ends being tethered to other two blocks and the mismatch of the cross-section areas at the PE−PEO and PEO−P5T interfaces (see Appendix). The structure of the lamellar morphology in EEO−P5T continues to change with the fourth-order diffraction peak gradually vanishing as the temperature decreases (Figure 4A). The change in the overall long spacing, L, is plotted as a function of temperature in Figure 5. A monotonic decrease in the L is seen with the onset of a slight kink at 25 °C, which may suggest a phase transition in the sample.

The crystalline morphology was also studied by PLM. When the sample was slowly cooled from isotropic melt to 88 °C, the PLM texture is shown in Figure 6. Even though the sample was annealed for a long time at 88 °C, no texture of regular spherulitic crystals was observed. This suggests that the introduction of the discotic block hindered the growth of regular spherulitic morphology. When the sample was further cooled, no obvious change in the texture could be detected at temperatures below the transition temperature of 23 °C.

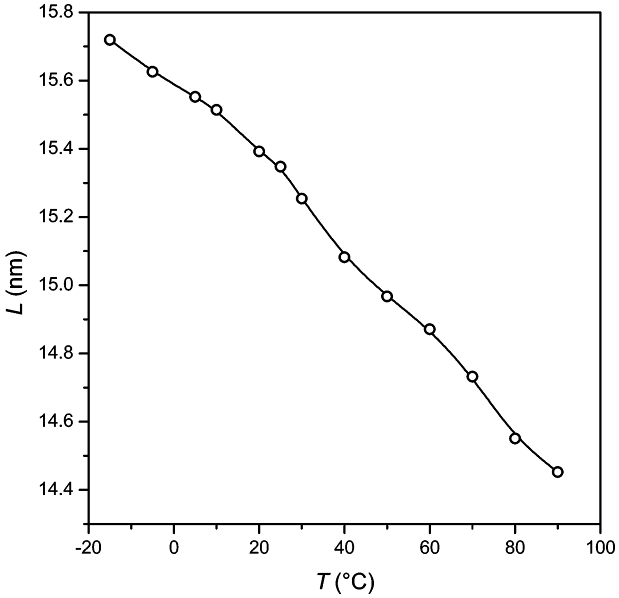

Figure 5. Overall *d*-spacing changes as a function of temperature.

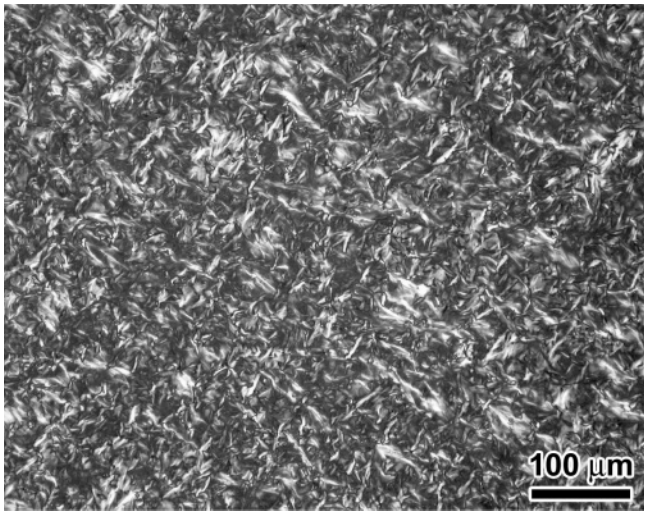

Figure 6. Typical PLM micrograph of EEO−P5T annealed at 88 °C for 20 min after cooled down from an isotropic melt at 1 °C/min.

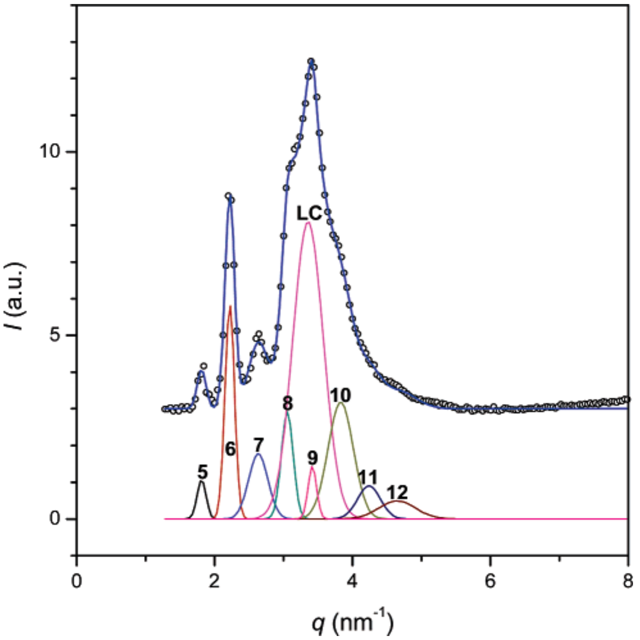

Figure 7. Peak deconvolution for the WAXD profile in the low-angle region at −15 °C. The open symbols are experimental data, and the solid lines are Gaussian functions. The regression coefficient is 0.998. The reflections from the crystalline lamellae and the discotic liquid crystalline structure are also labeled.

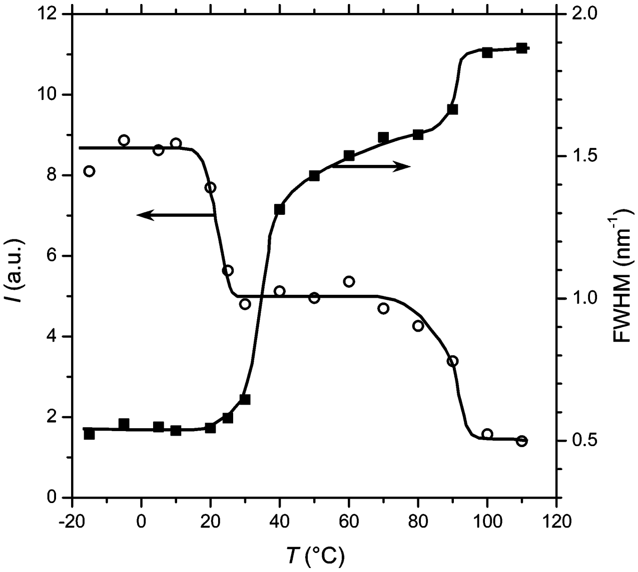

Figure 8. Intensity and fwhm of the fitted discotic liquid crystalline peak (at q = 3.4 ∼ 3.7 nm^{-1}) as functions of temperature.

The changes of the scattering profiles in the low-angle region (1−7 nm^{-1}) in Figure 4B correlate well with the phase transitions observed by DSC. To reveal the detail of the changes, the peak intensity and the width of the liquid crystalline reflections were analyzed. However, as mentioned above, these broad scattering peaks overlapped with higher-order lamellar scattering peaks and needed to be separated. Peak deconvolutions were performed using the Peakfit 4.0 software. Example results from the WAXD profile at −15 °C are shown in Figure 7, where symmetric Gaussian functions are used for all peaks. After deconvolution, a broad peak for the liquid crystalline reflection was obtained. When the scattering intensity of these low-angle peaks is plotted as a function of temperature, a two-step change is seen in Figure 8. The first transition occurs around 20 °C, and the second transition occurs at 93 °C. These transitions correlate well with the DSC results. The full width at half-maximum (fwhm) for these broad peaks is also plotted as a function of temperature in Figure 8. Two transitions in the fwhm curve are seen at ca. 35 and 93 °C. In the fwhm curve, the lower transition (at 35 °C) occurs at a slightly higher temperature than that in the intensity curve (20 °C), while the higher transition temperatures from both curves are similar. This may be due to the fact that the lower temperature transition is relatively broad (see DSC curve in Figure 3), where the fwhm approach is less sensitive to probe the structure changes than the intensity approach (we note that the fwhm also reflects the correlation length of an ordered structure).

Phase Identification by 2D Simultaneous SAXS and WAXD Studies. To identify different crystalline and liquid crystalline phases, 2D SAXS and WAXD experiments have been carried out, and results are shown in Figure 9. Parts A and B of Figure 9 represent

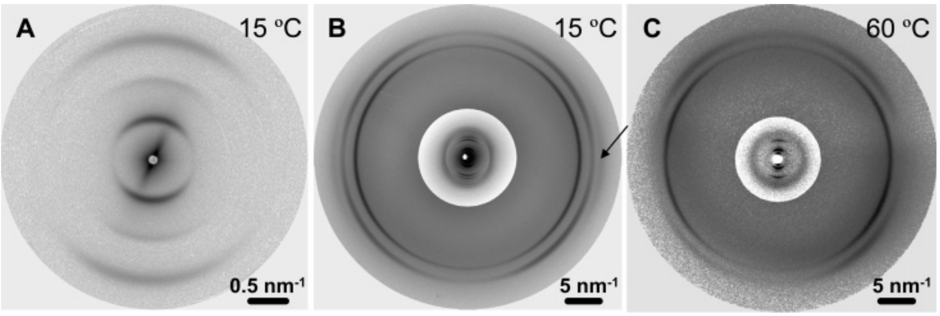

Figure 9. 2D SAXS and WAXD scattering patterns of shear-oriented EEO−P5T at different temperatures: (A) SAXS and (B) WAXD at 15 °C and (C) WAXD at 60 °C. The intensities are in logarithmic scales. The contrast at low-angle regions of WAXD patterns is adjusted for clarity.

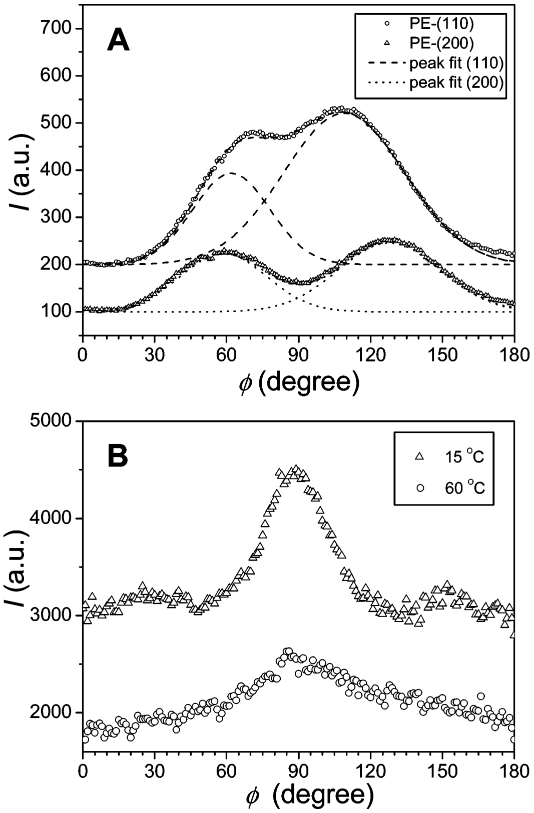

Figure 10. Azimuthal profiles extracted from the 2D WAXD patterns in Figure 9B,C of shear-oriented EEO−P5T: (A) PE (110) and (200) azimuthal profiles at 15 °C and (B) azimuthal profiles for the liquid crystalline reflections at $q = 3.4{-}3.6$ nm^{-1} at 15 and 60 °C. The dashed and dotted lines are the best fits using Gaussian functions. Curves are overlaid for clarity.

the 2D SAXS and WAXD patterns for a shear-oriented EEO−P5T sample at 15 °C, respectively. Three orders of lamellar reflections are seen on the meridian in Figure 9A, indicating the PE crystalline lamellae are aligned horizontally. The 3rd (very strong), 6th (strong), 7th (strong), 8th (weak), and even 9th (very weak) orders of reflections on the meridian are also seen in the low-angle region in Figure 9B. The PE crystal orientation in the crystalline lamellae can be studied from the orientation of (110) and (200) reflections in the quadrant.[18b] Azimuthal profiles extracted from both (110) and (200) reflections are shown in Figure 10A. Two maxima are observed at azimuthal angles of 62° and 108°, respectively, for the PE (110) reflection, indicating the existence of a tilt angle of 23° from the lamellar normal. Note that asymmetric reflection intensities may originate from the slight misalignment of the sample with respect to the incident X-ray beam. This value is similar to our previous report of EEO oligoblock copolymers[18b] and other reports of long alkanes.[24] Similarly, the PE (200) reflections also exhibited two maxima at 59° and 128° in the azimuthal profile. Supposedly, these two maxima should occur at the same angles as those of the (110) reflections (e.g., in the PE fiber pattern[25]). The reason for the slight difference in the azimuthal angle may be due to the sample misalignment and/or experimental errors.

The discotic liquid crystalline phase can be identified from a pair of relatively sharp reflections on the equator at $q = 3.4$ nm^{-1} (d-spacing = 1.85 nm) in Figure 9B. Another pair of weak reflections at $q = 17.7$ nm^{-1} (indicated by the arrow in Figure 9B) are observed on the equator with a d-spacing of 0.35 nm. This weak peak is also indicated by the arrows in the 1D WAXD profiles in Figure 4B. These observations suggest a columnar phase for the P5T blocks, confined between PE crystalline lamellae. The vertical streaks from this liquid crystalline diffraction indicate the bilayer nature of the sandwiched columns, which have almost no correlation in the lamellar normal direction. Whether this columnar phase is a laterally ordered columnar phase or a nematic phase should be judged from the following facts. First, no higher-order reflections are observed in the 2D WAXD pattern. Second, the fwhm is approximately 0.52−0.64 nm^{-1}, which is much broader than those of 0.01−0.02 nm^{-1} for typical hexagonal columnar phases.[26] A typical nematic phase has a fwhm of 0.7 nm^{-1},[27] which is close to our observations. Therefore, we assign this columnar phase as N_{col}. This determination is similar to the one reported before for a side-chain discotic liquid crystalline copolymer.[28] A schematic representation is shown in Figure 11A, where the PE chains are tilted at 23° with respect to the lamellar normal. In Figure 11A, the 2D nematic columns on the left assembly were arranged out of the paper, resulting in inter-columnar reflections at $q = 3.4$ nm^{-1} on the equator, while those on the right assembly would result in interdiscotic reflections at $q = 17.7$ nm^{-1} on the equator.

When the temperature increases to 60 °C, 2D WAXD patterns for the sheared sample are shown in Figure 9C. The horizontal orientation of the PE lamellae is retained as shown by the low-angle lamellar reflections on the meridian. A diffuse reflection ring is seen at $q = 3.6$ nm^{-1} (d-spacing = 1.74 nm, which is the average distance between neighboring discotic molecules), and no reflection is seen at $q = 17.7$ nm^{-1}. These observations suggest the presence of a N_D phase for the P5T blocks sandwiched between neighboring PE crystalline lamellae. As shown in Figure 10B, the azimuthal scan

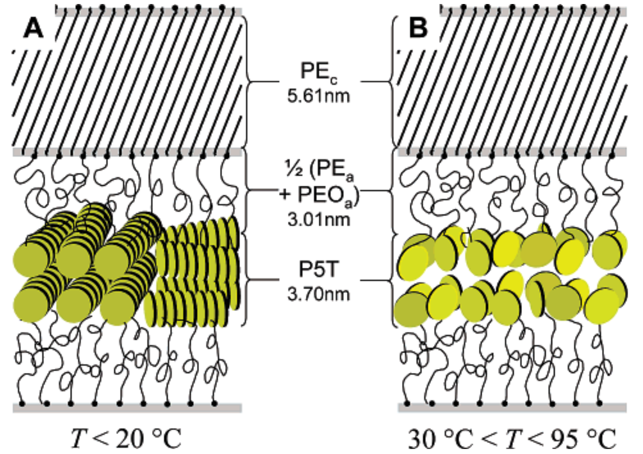

Figure 11. Schematics of the EEO−P5T at different temperatures. (A) Below 20 °C: interdigitated, single-layer crystalline PE, amorphous PEO, and bilayer N_{col} P5T. (B) Between 30 and 90 °C: interdigitated, single-layer crystalline PE layer, amorphous PEO layer, and bilayer N_D P5T.

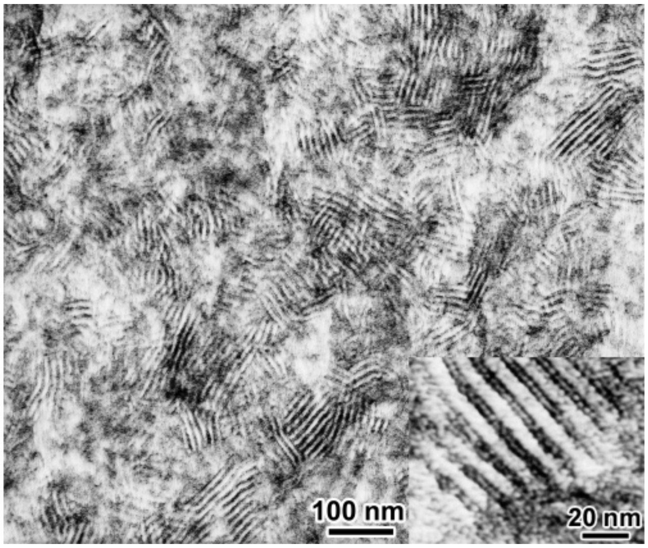

Figure 12. TEM micrograph of a thin EEO−P5T section stained with RuO_4. The inset shows a high-magnification micrograph.

profile of the reflection at $q = 3.6$ nm^{-1} shows a broad maximum at ca. 90° (on the equator), suggesting a relatively parallel orientation of the P5T disks with respect to the lamellar normal. However, the degree of orientation in the discotic molecules is much less than that of columnar orientation, as judged from the fwhm values of the azimuthal profiles for the N_{col} at 15 °C (29°) and N_D at 60 °C (78°). A schematic representation is shown in Figure 11B.

The ABC three-layered lamellar morphology proposed in Figure 11 is further confirmed by the TEM study. As shown in Figure 12, the lamellar structure in the triblock oligomer is observed, in which the bright layers represent the PE lamellar crystals (not stained) and the dark layers are the PEO blocks (stained). We notice that the average grain size of the lamellar structure is only ca. 100 nm, which is much smaller than that in the parent PE-*b*-PEO diblock copolymers.[18b] A high-magnification TEM micrograph in the inset of Figure 12 shows detailed morphology of the lamellae structure. Light gray lines between the dark PEO layers can be clearly seen, which represent the P5T layers sandwiched between the amorphous PEO layers. Although the grain sizes are small, 10 or more layers of lamella stacking are often seen in the TEM micrograph. This lamella stacking of 10 or more layers could result in multiple X-ray diffractions as observed in the X-ray experiments.

From the above study, several phases were identified in EEO−P5T: (1) PE crystals, which melted at 93.8 °C; (2) a confined N_{col} phase in P5T, which transformed into a confined N_D phase at ca. 23 °C; (3) a confined N_D phase in P5T, which became isotropic as soon as the PE crystals melt. We believe that this is the first time that the isotropization (or the formation) of the N_D phase is induced by the melting (or crystallization) of the PE block crystals. It is speculated that after the PE crystals melt the amorphous PE blocks serve as an additional solvent, which can homogenize the liquid crystalline N_D phase to become isotropic.

Since the PE crystallinity was 81 wt %, there should be 11.2 carbons in the amorphous melt and 47.8 carbons in the crystals, assuming every chain crystallizes. According to our previous report,[18b] the PE crystal thickness (with 47.8 carbons), $d_{PE,c}$, was estimated to be 5.61 nm, taking into account of the chain tilting angle of 23°. The thickness of one amorphous PE-PEO layer can be calculated using the method described in the Appendix. Generally, a pyramidal frustum is assumed for a covalently bonded amorphous PE−PEO chain with the amorphous PE connecting to a PE lamellar crystal and the amorphous PEO linking to a P5T discotic molecule. The top area of the frustum is 0.4 nm^2, which is the area of one unit cell of PE crystal divided by cos 23° due to chain tilt. The bottom area of the frustum is 0.647 nm^2, assuming a rectangular area among neighboring discotic molecules (i.e., 1.85 nm × 0.35 nm) in the N_{col} phase. Assuming the densities are the same as bulk amorphous PE and PEO (0.825 and 1.061 g/cm^3,[18b] respectively), the thickness of an amorphous PE−PEO layer can be calculated to be 3.01 nm. Assuming a double-layered P5T phase is sandwiched between the amorphous PEO layers, the thickness of the P5T is approximately twice the distance between the neighboring P5T columns (1.85 nm), i.e., 3.70 nm. Adding all these layer thicknesses, a total thickness of 15.33 nm was obtained for the N_{col} phase in EEO−P5T. This is very close to the overall layer spacing observed at 25 °C (15.35 nm) in Figure 5. Therefore, the columnar and discotic models in Figure 11 are reasonable representations based on our experimental results. From this calculation, we notice a nonuniform stretching of the amorphous PE and PEO chains at each end connecting to the PE crystals and P5T molecules (basal area of 0.4 nm^2 vs 0.647 nm^2), respectively. As the PE crystals grow laterally, unbalanced stress will accumulate to destabilize the growth. Because of a symmetric arrangement of different layers [PE-PEO−(P5T/P5T)−PEO−PE, see Figure 11], no lamellae bending will be expected. A reasonable option is that the PE crystals have to break from time to time, and the grain sizes of the lamellar structure are thus small. This may explain the small grain sizes we have observed in the TEM experiments (see Figure 12).

Conclusions

In summary, an oligomeric PE-*b*-PEO-*b*-P5T triblock copolymer has been successfully synthesized, where the PE blocks are crystalline, the PEO blocks retain in the amorphous state, and the P5T blocks form discotic liquid crystalline phases sandwiched between amorphous PEO layers. Discotic liquid crystalline phases of P5T are identified by 2D WAXD experiments: (1) an N_{col} phase below 23 °C; (2) an N_D phase between 30 and 90 °C. The isotropization of the N_D phase is induced by the melting of PE lamellar crystals, since the molten PE blocks serve as a solvent to homogenize the N_D phase after PE crystals melt. Because of the mismatch of the basal areas (per PEO chain) at the PE crystal/amorphous PE and PEO/columnar P5T interfaces, unbalanced stresses could accumulate as the PE crystals grow laterally. As a result, the grain size of the crystalline lamellar morphology is relatively small (ca. 100 nm) as compared to the neat PE-*b*-PEO diblock copolymers.

Acknowledgment. This work was supported by the startup fund provided by University of Connecticut, NSF CAREER Award DMR-0348724, and 3M Nontenured Faculty Award. The synchrotron SAXS experiments were carried out in the National Synchrotron Light Source, Brookhaven National Laboratory, supported by the DOE (Grant DE-FG02-99ER 45760).

Appendix

Since one PE end of the amorphous part of PE-*b*-PEO is linked to PE crystals and the other PEO end is linked to P5T molecules, the amorphous part of PE-*b*-PEO, presumably, occupies a pyramidal frustum (see Figure 13A). Because the PE chains are interdigitated in the crystals, the top area, A_t, can be estimated as

$$A_t = 2a_{PE}/\cos 23° \qquad (1)$$

where a_{PE} is the area per PE chain in the crystals (0.183 nm^2).[18b] Since P5T molecules are not interdigitated in the N_{col} phase, the bottom area, A_b, equals the rectangular area among four neighboring P5T molecules in two adjacent columns (see Figure 13B):

$$A_b = d_{inter}d_{intra} \qquad (2)$$

where d_{inter} is the distance between columns (1.85 nm) and d_{intra} is the intra-column distance (i.e., between neighboring disks within a column, 0.35 nm).

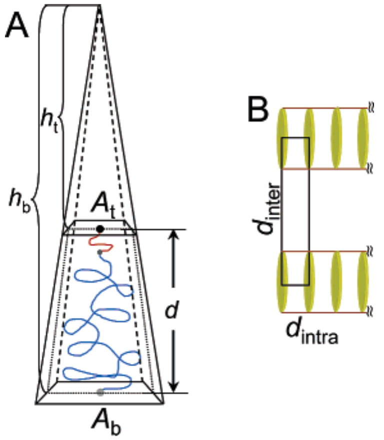

Figure 13. (A) Schematic representation of the pyramidal frustum for the amorphous part of the EEO chain. (B) Schematic representation of a top view of the N_{col} phase. The rectangular area among four neighboring P5T disks in two adjacent columns is assumed as the basal area for one PEO chain.

Assuming the density of amorphous PE and PEO in the diblock copolymer is the same as those for bulk samples (0.825 and 1.061 g/cm^3, respectively), the volume of the amorphous part of PE-*b*-PEO can be evaluated as

$$V = M_{PE,a}/\rho_{PE,a} + M_{PEO,a}/\rho_{PEO,a} \qquad (3)$$

where $M_{PE,a}$ is half of the molecular weight in the amorphous part of the PE block (see Figure 11, 5.6 carbons or 78.4 g/mol) and $M_{PEO,a}$ is the molecular weight of the PEO block (896 g/mol). Assuming the pyramidal frustum is the difference of two pyramids (Figure 13A), the two heights of these pyramids are h_t and h_b, respectively. The ratio of h_t/h_b is

$$h_t/h_b = \sqrt{A_t/A_b} \qquad (4)$$

and the volume can be calculated as

$$V = {}^1/_3(A_bh_b - A_th_t) \qquad (5)$$

From eqs 4 and 5, the thickness of the amorphous PE and PEO layer is the height of the pyramidal frustum, i.e., $d = h_b - h_t$.

References and Notes

(1) Lehn, J.-M. *Supramolecular Chemistry*; VCH: Weihheim, 1995.
(2) Tschierske, C. *Annu. Rev. Prog. Chem., Sect. C* **2001**, *97*, 191.
(3) Tschierske, C. *Prog. Polym. Sci.* **1996**, *21*, 775.
(4) Seddon, J. M.; Templer, R. M. In *Handbook of Biological Physics*; Lipowsky, R., Sackmann, E., Eds.; Elsevier: Amsterdam, 1995; Vol. 1, p 97.
(5) Ober, C. K.; Wegner, G. *Adv. Mater.* **1997**, *9*, 17.
(6) Hamley, I. W. *The Physics of Block Copolymers*; Oxford University Press: Oxford, 1998.
(7) Lee, M.; Cho, B. K.; Zin, W. C. *Chem. Rev.* **2001**, *101*, 3869.
(8) Chen, J. T.; Thomas, E. L.; Ober, C. K.; Hwang, S. S. *Macromolecules* **1995**, *28*, 1688. (b) Chen, J. T.; Thomas, E. L.; Ober, C. K.; Mao, G.-P. *Science* **1996**, *273*, 343. (c) Thomas, E. L.; Chen, J. T.; O'Rourke, M. J.; Ober, C. K.; Mao, G. *Macromol. Symp.* **1997**, *117*, 241.
(9) Lee, M.; Cho, B.-K.; Kim, H.; Yoon, J.-Y.; Zin, W.-C. *J. Am. Chem. Soc.* **1998**, *120*, 9168. (b) Lee, M.; Cho, B.-K.; Kim, H.; Zin, W.-C. *Angew. Chem., Int. Ed.* **1998**, *37*, 638. (c) Lee, M.; Cho, B.-K.; Jang, Y.-G.; Zin, W.-C. *J. Am. Chem. Soc.* **2000**, *122*, 7449. (d) Lee, M.; Lee, D.-W.; Cho, B.-K. *J. Am. Chem. Soc.* **1998**, *120*, 13258.
(10) Stupp, S. I.; LeBonheur, V.; Walker, K.; Li, K. S.; Huggins, K. E.; Keser, M.; Amstutz, A. *Science* **1997**, *276*, 384. (b) Pralle, M. U.; Urayama, K.; Tew, G. N.; Neher, D.; Wegner, G.; Stupp, S. I. *Angew. Chem., Int. Ed.* **2000**, *39*, 1486. (c) Zubarev, E. R.; Pralle, M. U.; Li, L.; Stupp, S. I. *Science* **1999**, *121*, 9852.
(11) Jenekhe, S. A.; Chen, X. L. *Science* **1998**, *279*, 1903. (b) Chen, X. L.; Jenekhe, S. A. *Langmuir* **1999**, *15*, 8007.
(12) Zhong, X. F.; Francois, B. *Macromol. Chem. Rapid Commun.* **1998**, *9*, 411. (b) Widawski, G.; Rawiso, M.; Francois, B. *Nature (London)* **1994**, *369*, 387. (c) Francois, B.; Pitois, O.; Francois, J. *Adv. Mater.* **1995**, *7*, 1041.
(13) Otmakhova, O. A.; Kuptsov, S. A.; Talroze, R. V.; Patten, T. E. *Macromolecules* **2003**, *36*, 3432.
(14) Thunemann, A. F.; Kubowicz, S.; Burger, C.; Watson, M. D.; Tchebotareva, N.; Mullen, K. *J. Am. Chem. Soc.* **2003**, *125*, 352.
(15) Abeysekera, R.; Bushby, R. J.; Caillet, C.; Hamley, I. W.; Lozman, O. R.; Lu, Z.; Robards, A. W. *Macromolecules* **2003**, *36*, 1526.
(16) Li, C. Y.; Teneti, K. K.; Zhang, D.; Zhang, H.; Wan, X.; Chen, E.; Zhou, Q. F.; Carlos, A.-O.; Sics, I.; Hsiao, B. S. *Macromolecules* **2004**, *37*, 2854.
(17) Clarkson, G. J.; Cook, A.; McKeown, N. B.; Treacher, K. E.; Ali-Adib, Z. *Macromolecules* **1996**, *29*, 913.
(18) Sun, L.; Liu, Y.; Zhu, L.; Hsiao, B. S.; Avila-Orta, C. A. *Macromol. Rapid Commun.* **2004**, *25*, 853. (b) Sun, L.; Liu, Y.; Zhu, L.; Hsiao, B. S.; Avila-Orta, C. A. *Polymer* **2004**, *45*, 8181−8193.

(19) Allen, M. T.; Diele, S.; Harris, K. D. M.; Hegmann, T.; Kariuki, B. M.; Lose, D.; Preece, J. A.; Tschierske, C. *J. Mater. Chem.* **2001**, *11*, 301.

(20) Boden, N.; Borner, R. C.; Bushby, R. J.; Cammidge, A. N.; Jesudason, M. V. *Liq. Cryst.* **1993**, *15*, 851.

(21) Kumar, S.; Manickam, M. *Synthesis* **1998**, 1119.

(22) Trent, J. S.; Scheinbeim, J. I.; Couchman, P. R. *Macromolecules* **1983**, *16*, 589.

(23) For example, the melting peak can be deconvoluted into two peaks: a peak at 90.6 °C having 79.3% of the total peak area and the other at 93.6 °C with 20.7% of the total peak area. The heat of fusion (ΔH_f) of the whole peak is 81 J/g as measured by DSC. So, the ΔH_f values are 64.1 and 16.7 J/g for both peaks, respectively. Judging from the magnitude of ΔH_f, we could only assign the PE melting to the lower melting peak (90.6 °C) and the N_D−I transition to the higher melting peak (93.6 °C). After normalization to the P5T weight fraction, the N_D−I transition has a ΔH_f of 50.1 J/g. This value is quite high for a typical nematic transition and is much higher than the one reported for a N_D−I transition (0.33 J/g or 0.3 kJ/mol) in ref 28.

(24) Ungar, G.; Zeng, X. B. *Chem. Rev.* **2001**, *101*, 4157.

(25) Zugenmaier, P.; Cantow, H. J. *Kolloid Z. Z. Polym.* **1969**, *230*, 229.

(26) Ramos, L.; Molino, F. *Phys. Rev. Lett.* **2004**, *92*, 018301.

(27) Schröder, M. W.; Diele, S.; Pelzl, G.; Dunemann, U.; Kresse, H.; Weissflog, W. *J. Mater. Chem.* **2003**, *13*, 1877.

(28) Kouwer, P. H. J.; Jager, W. F.; Mijs, W. J.; Picken, S. J. *Macromolecules* **2000**, *33*, 4336.

MA047590W